Cryo-EM structures elucidate neutralizing mechanisms of anti-chikungunya human monoclonal antibodies with therapeutic activity

Feng Long[a], Rachel H. Fong[b], Stephen K. Austin[c], Zhenguo Chen[a], Thomas Klose[a], Andrei Fokine[a], Yue Liu[a], Jason Porta[a], Gopal Sapparapu[d], Wataru Akahata[e], Benjamin J. Doranz[b], James E. Crowe Jr.[d,f,g], Michael S. Diamond[c], and Michael G. Rossmann[a,1]

[a]Department of Biological Sciences, Purdue University, West Lafayette, IN 47907; [b]Integral Molecular, Inc., Philadelphia, PA 19104; [c]Departments of Medicine, Molecular Microbiology, Pathology, and Immunology, Washington University School of Medicine, St. Louis, MO 63110; [d]Department of Pediatrics, Vanderbilt University, Nashville, TN 37232; [e]VLP Therapeutics, LLC, Gaithersburg, MD 20878; [f]Departments of Pathology, Microbiology, and Immunology, Vanderbilt University, Nashville, TN 37232; and [g]Vanderbilt Vaccine Center, Vanderbilt University Medical Center, Vanderbilt University, Nashville, TN 37232

Edited by Peter Palese, Icahn School of Medicine at Mount Sinai, New York, NY, and approved October 1, 2015 (received for review August 5, 2015)

Chikungunya virus (CHIKV) is a mosquito-transmitted alphavirus that causes severe acute and chronic disease in humans. Although highly inhibitory murine and human monoclonal antibodies (mAbs) have been generated, the structural basis of their neutralizing activity remains poorly characterized. Here, we determined the cryo-EM structures of chikungunya virus-like particles complexed with antibody fragments (Fab) of two highly protective human mAbs, 4J21 and 5M16, that block virus fusion with host membranes. Both mAbs bind primarily to sites within the A and B domains, as well as to the B domain's β-ribbon connector of the viral glycoprotein E2. The footprints of these antibodies on the viral surface were consistent with results from loss-of-binding studies using an alanine scanning mutagenesis-based epitope mapping approach. The Fab fragments stabilized the position of the B domain relative to the virus, particularly for the complex with 5M16. This finding is consistent with a mechanism of neutralization in which anti-CHIKV mAbs that bridge the A and B domains impede movement of the B domain away from the underlying fusion loop on the E1 glycoprotein and therefore block the requisite pH-dependent fusion of viral and host membranes.

chikungunya virus-antibody complexes | cryo-electron microscopy structure | neutralizing mechanism | viral fusion inhibition

Chikungunya virus (CHIKV) is an enveloped, positive-stranded RNA virus that belongs to the alphavirus genus of the Togaviridae family (1, 2). CHIKV is transmitted to humans by *Aedes* species mosquitoes and causes a debilitating febrile illness associated with acute and chronic arthritis (3, 4). Since the first human CHIKV infection was reported in East Africa in 1952 (5), epidemics of CHIKV have occurred in Africa, Asia, and Europe (6, 7). A CHIKV outbreak in the Caribbean area in late 2013 spread through the Americas and caused about 1.4 million infections (8). Despite its global disease burden and risk of spread, there is no available vaccine or effective antiviral drug for CHIKV.

The genome of CHIKV is ∼11.8 kb long and encodes nine viral proteins, five of which are structural (capsid, E3, E2, 6K, and E1) (2). These structural proteins are translated as a single polyprotein, which is then cleaved into the capsid, p62, 6K, and E1 proteins by cellular and viral proteases. During maturation, p62 is cleaved to release E3, which protects the fusion loop in the immature virus. The virus consists of a central core with diameter of ∼400 Å with the icosahedrally organized capsid proteins surrounding the viral genome. The nucleocapsid core is enveloped by a lipid membrane into which the E1 and E2 glycoproteins are inserted (9). The mature CHIKV particle has a diameter of 700 Å. The E2 glycoprotein binds to uncharacterized cellular receptors to initiate virus entry into host cells, whereas E1 glycoprotein participates in virus–host cell membrane fusion (10, 11). Although the E3 and 6K proteins contribute to virus assembly and maturation, they are released during the formation of mature CHIKV (12–14). Nevertheless, E3 remains associated with the mature virus in some alphaviruses, including Semliki Forest (SFV) and Venezuelan equine encephalitis (VEEV) viruses (15, 16).

Virus-like particles (VLPs) are noninfectious recombinant particles that resemble native virus but lack viral genomes. As VLPs can be highly immunogenic and safe to work with under lower biocontainment levels, they have been used widely in the development of vaccines, gene therapy vectors, and other studies (17, 18). VLP-based vaccines are currently commercialized for hepatitis B virus and human papillomavirus (19). Indeed, a VLP-based vaccine against CHIKV is immunogenic and protective (20) and has advanced through phase 1 clinical trials in humans (21).

A cryo-EM structure of CHIKV VLPs has been determined to 5.3-Å resolution (22). Like other alphaviruses, CHIKV is icosahedral and has T = 4 quasi-symmetry (Fig. 1*A*). The nucleocapsid core consists of 12 pentamers around each fivefold vertex and 30 hexamers around each icosahedral twofold axis. The outer surface of mature CHIKV particles is comprised of 80 spikes. Each spike is formed by three copies of an E1–E2 heterodimer. There are 20 icosahedral (i3) spikes sitting on the icosahedral threefold axes and 60 quasi-threefold (q3) spikes in general quasi-threefold positions.

Significance

A recent outbreak of chikungunya virus in the Americas has caused more than one million infections in humans. The reemergence of this virus has become a major threat to public health due to a lack of available vaccines and antiviral drugs. We determined the cryo-EM structures of chikungunya virus particles complexed with two of the most potent human antibody fragments described in a previous study. Both antibodies neutralized the virus by stabilizing the position of the viral surface glycoproteins, which blocks the exposure of the glycoprotein fusion loops required to initiate viral entry into the cytoplasm of a target cell.

Author contributions: F.L., B.J.D., J.E.C., M.S.D., and M.G.R. designed research; F.L., R.H.F., S.K.A., Z.C., Y.L., G.S., and W.A. performed research; F.L., R.H.F., S.K.A., Z.C., T.K., A.F., J.P., B.J.D., J.E.C., M.S.D., and M.G.R. analyzed data; and F.L., B.J.D., J.E.C., M.S.D., and M.G.R. wrote the paper.

The authors declare no conflict of interest.

This article is a PNAS Direct Submission.

Data deposition: The atomic coordinates and structure factors of the 4J21 and 5M16 Fab fragments have been deposited in the Protein Data Bank, www.pdb.org (PDB ID codes 5CGY and 5CHN, respectively). The cryo-EM density maps of CHIKV VLPs in complex of the 4J21 and 5M16 Fab fragments have been deposited in the EM Data Bank (accession nos. EMD-3148 and EMD-3149, respectively).

[1]To whom correspondence should be addressed. Email: mr@purdue.edu.

This article contains supporting information online at www.pnas.org/lookup/suppl/doi:10.1073/pnas.1515558112/-/DCSupplemental.

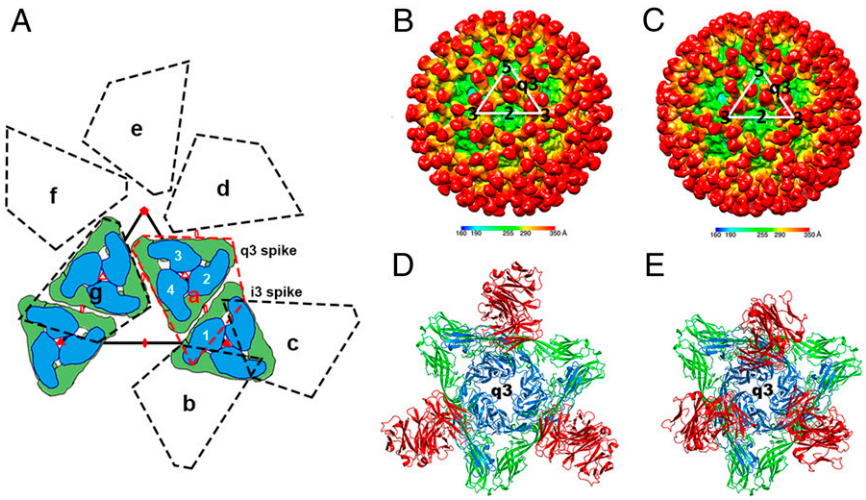

Fig. 1. Cryo-EM structures of the CHIKV VLPs in complex with Fab fragments of 4J21 and 5M16. (*A*) Diagrammatic representation of the q3 and i3 spikes according to T = 4 icosahedral symmetry. The regions (a–g) enclosed in dashed lines represent seven icosahedral asymmetric units. The white numbers (1–4) indicate the four independent quasi-equivalent positions of the E1 (green)–E2 (blue) heterodimer in one icosahedral asymmetric unit. The icosahedral and quasi symmetry elements are respectively shown as filled and unfilled triangles, pentagons or ellipses. (*B* and *C*) The cryo-EM reconstructions of the virus-Fab (4J21, *B* and *D*; 5M16, *C* and *E*) complexes are colored according to the radial distance of the surface from the viral center. The white triangles denote boundaries of an icosahedral asymmetric unit. (*D* and *E*) Ribbon drawings of the q3 spike with the bound Fab. E1 is shown in green, E2 is in blue, and the Fab is in red.

Thus, in each icosahedral asymmetric unit, there is one q3 spike and one-third of an i3 spike.

The structure of alphavirus E1 (23) is similar to that of the E glycoprotein of flaviviruses (24) and consists of three domains, E1-I, E1-II, and E1-III. E1-I is an eight-stranded barrel with up and down topology. E1-II is inserted into domain I and forms the dimerization region of the homologous protein in flaviviruses. E1-III has an Ig-like fold. The structure of E2 was determined by Voss et al. (25) who crystallized the E1-E2 heterodimer of CHIKV and by Li et al. (26) who crystallized an $(E1\text{-}E2)_3$ trimeric spike of Sindbis virus (SINV). The structure of E2 also has three domains, E2-A, E2-B, and E2-C, and a β-ribbon connector. The E2-A domain contains the putative receptor binding site (22, 26, 27). The fusion loop in E1-II is covered by the E2-B domain at neutral pH but becomes exposed for membrane fusion in an acidic environment (25, 26).

Many monoclonal antibodies (mAbs) that neutralize CHIKV infection recognize epitopes on the solvent-accessible surface of the E2 protein (28–32). The only previous structural studies of CHIKV–antibody complexes were of four neutralizing murine mAbs. Three of these antibodies (m10, m242, and CHK-9) bound to the putative receptor binding sites, whereas one, CHK-152, inhibited the exposure of the fusion loop by immobilizing the E2-B domain (22). Analogous structural studies have been reported for other alphaviruses, such as Ross River virus (27), Sindbis virus (33), and VEEV (34). However, there are no published structures of CHIKV in complex with human antibodies.

Here, we report the cryo-EM structures of CHIKV VLPs in complex with the Fab fragments of two highly neutralizing and protective human mAbs: 4J21 and 5M16. Both mAbs were isolated from a CHIKV-immune donor and were shown to have therapeutic activity in immunodeficient mice lacking type I IFN signaling (35). Although the previous functional studies showed that both these antibodies blocked virus fusion with host membranes, we now establish the structural basis for this inhibition. To accomplish this, we determined the crystal structures of these Fab fragments, which were then used to help interpret the ∼15-Å resolution structures of the cryoEM Fab–virus complexes. The

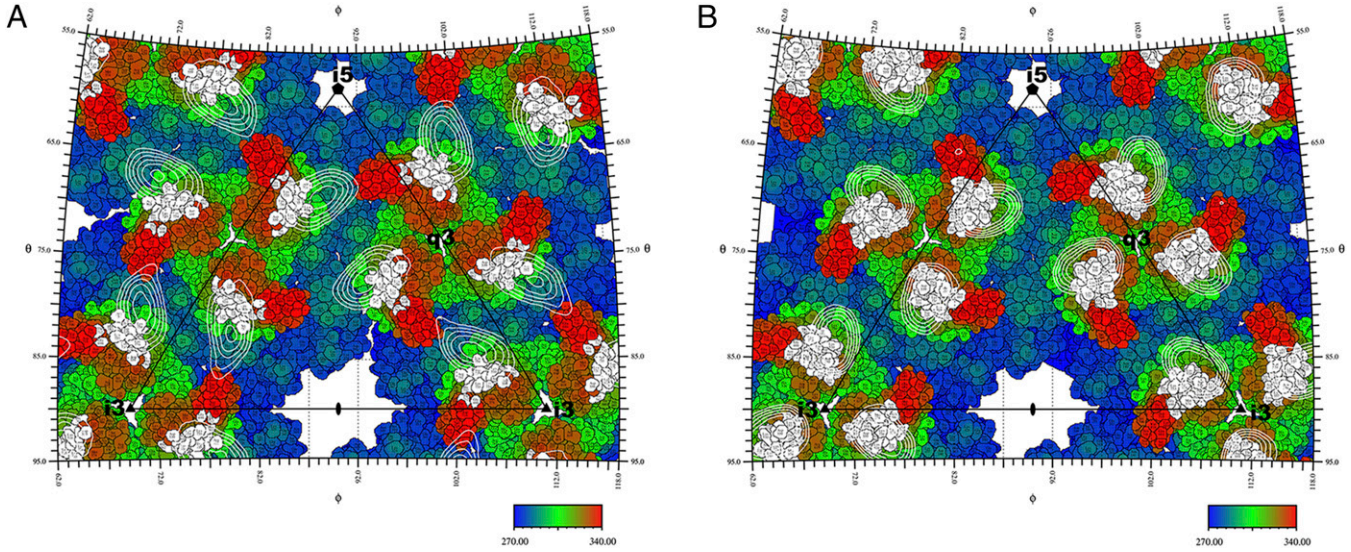

Fig. 2. Roadmaps showing the projected surfaces of the CHIKV VLP-4J21 and VLP-5M16 complexes, colored according to the radial distance of the surface from the center of the respective particles. The black triangles denote boundaries of the icosahedral asymmetric unit. The projections of the Fab molecules (4J21, *A*; 5M16, *B*) onto the surfaces of the VLPs are represented by white contours. The residues in the Fab footprints are shown in white. The roadmaps were created by the program RIVEM (48).

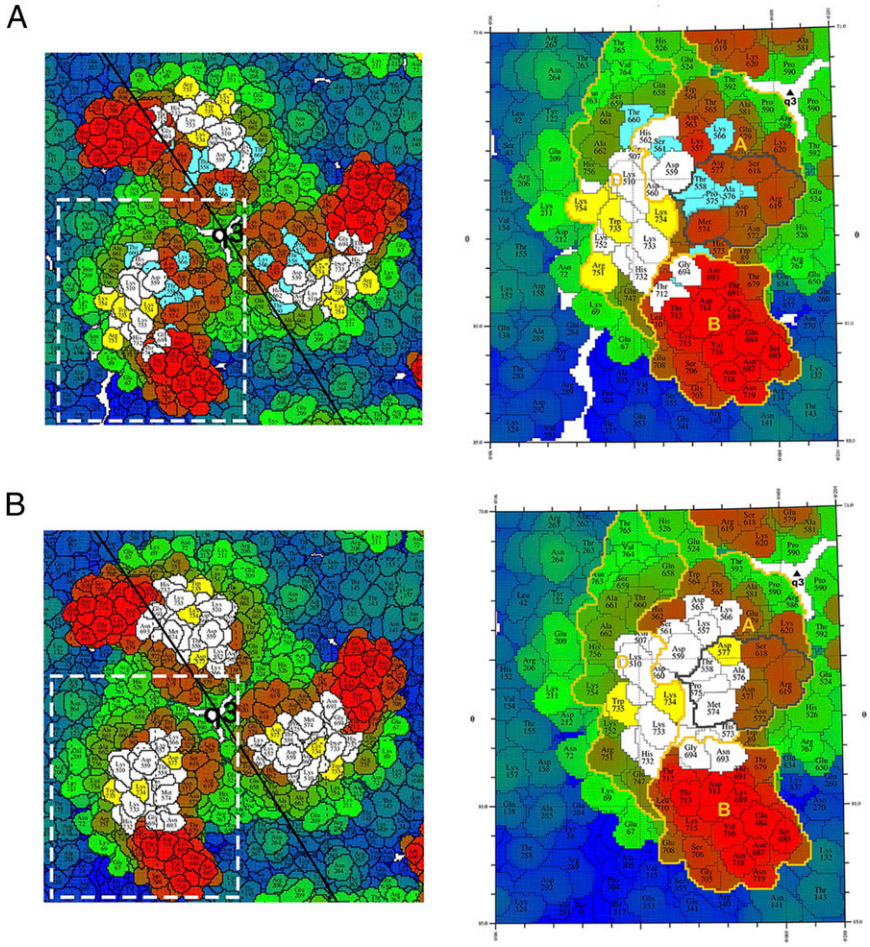

Fig. 3. Enlargement of the quasi-threefold spike to show the footprints of the antibodies 4J21and 5M16. The roadmaps are colored radially with respect to the virus center, with the smallest radius in blue and the largest radius in red. The cryo-EM footprints of 4J21 (*A*) and 5M16 (*B*) are shown in white and yellow, the alanine scanning footprints are shown in baby blue and yellow, with yellow representing the common residues between two methods. The A, B domains and β-ribbon connector of E2 are labeled and outlined in gold. The putative receptor binding site is outlined with a black line.

resultant pseudo-atomic resolution structures show that these human mAbs share a binding footprint that bridges across the A and B domains on the E2 protein and prevent the B domain from moving away to expose the fusion loop.

Results and Discussion

Reconstruction of CHIKV VLPs in Complex with Fab Fragments. Two human mAbs, 4J21 and 5M16 (both IgG1 isotype), were selected for structural studies. These two mAbs had potent neutralizing activity, blocked viral fusion with host membranes, and had therapeutic activity in immunodeficient mice (35). The purified Fab molecules formed stable complexes with CHIKV VLPs. The bound antibody moieties could be recognized easily as branches on the surface of the VLPs cryo-electron density (Fig. 1 *B* and *C*). In both structures, there was one Fab fragment bound to each E1–E2 heterodimer. In each icosahedral asymmetric unit, there were three Fabs bound to the q3 spike and one Fab bound to the i3 spike. Thus, a total of 240 Fab molecules were bound per particle. However, the orientation and localization of the Fab fragments on the surface of the particles differed in the two Fab–VLP complexes (Fig. 1 *D* and *E*). The pseudo-twofold axes of the 5M16 Fabs are roughly radial to the virus, whereas the twofold axes of the 4J21 Fab make an angle of about 30° with the radial direction. As a result, one of the 4J21 Fabs on a q3 spike is close to a Fab on the neighboring i3 spike, whereas the other two Fabs on the q3 spike are each close to their neighboring fivefold related q3 spikes.

Crystal Structures of Fab Fragments. The crystal structures of the 4J21 and 5M16 Fab molecules were determined by X-ray crystallography to 2.3- and 2.1-Å resolution, respectively (Table S1). There were two Fab molecules in the asymmetric unit of the 4J21 crystals. The structures of the variable domains are almost identical in these two 4J21 Fab molecules (the RMS difference between equivalent Cα atoms between superimposed domains is 0.53 Å), but their elbow angles (219° and 234°) differ by 15°. The flexible elbow might facilitate antigen binding of the 4J21 antibody to the virus. The 5M16 Fab crystals also had two Fab molecules in one asymmetric unit. However, unlike 4J21, the two molecules are almost identical (the RMS difference between equivalent Cα atoms between superimposed molecules is 0.24 Å) and have the same elbow angle of 164°, suggesting that the elbow region is more flexible in the 4J21 Fab than in the 5M16 Fab.

Fitting of the E1–E2 Heterodimer Structure and Fab Structures into the Cryo-EM Densities. The crystal structures of CHIKV envelope proteins (E1–E2 heterodimer) and the 4J21 or 5M16 Fab fragments were fitted into the cryo-EM density maps of the VLP–Fab complexes, assuming T = 4 symmetry. The quality of fit was measured by the average of the density at all of the fitted atoms, "sumf". The densities at the grid points in the map were scaled by setting the

highest recorded density in the cryo-EM map to 100. As this procedure is rather arbitrary, it is only valid to compare the quality of fit for different domains within a map. Comparison between maps could be misleading if based on this criterion.

As the average height of the electron density measured by sumf for the virus and for the bound Fab molecules was similar (Tables S2 and S3), the antibody binding sites on the virus were fully occupied. The most obvious characteristic of the fitting results is that the density of the E2–B domain is lower for the 4J21 Fab complex compared with the cryo-EM density for the other E1 and E2 domains. A comparable reduction of the E2–B domain density was observed for the uncomplexed structure (22). This finding indicates that the B domain has greater flexibility relative to the other domains in the uncomplexed structure. The same observation was made in the crystallographic study of the E1–E2 heterodimer (25), where the temperature factor of the atoms in the B domain was about 56 $Å^2$ compared with about 40 $Å^2$ for the other atoms in the structure. Similarly, in the crystal structure of the $(E1–E2)_3$ trimers of SINV at pH 5.6, the B domains were disordered (26). The implication is that the B domain, which normally covers and protects the fusion loop in E1–DII, has greater flexibility than the rest of the structure. In contrast, the height of the E2–B density in the 5M16 complex is similar to all of the other domains (Table S4). Thus, in the VLP–5M16 complex, the B domain is stabilized by the bound Fab molecule, which impedes its movement away from the fusion loop. The stabilized B domain, in turn, prevents the exposure of the fusion loop on E1, which would inhibit fusion of the virus within a target host cell.

Interaction Between Fab and the Envelope Proteins. The footprint of both Fabs on the virus surface was defined by the atoms in the virus that were closer than 4 Å from any atom in the bound Fab molecule (Table S5). Fab 5M16 bound to the E2 A, and B domains and β-ribbon connector, whereas Fab 4J21 bound primarily to the E2 βr-ribbon connector (Figs. 2 and 3). The contact surface areas are 944 and 1277 $Å^2$ for the 4J21 and 5M16 Fab fragments, respectively. Presumably the larger area of contact of the B domain with the 5M16 Fab fragment, helped by its interaction with the β-ribbon connector, stabilizes the B domain in the complex with Fab 5M16. This mode of binding to the B domain suggests that the antibody 5M16 can neutralize the virus in part by inhibiting fusion, consistent with earlier observations according to an acid-bypass "fusion from without" assay (35).

Because both mAbs bind close to the putative receptor attachment site (22, 26), they also might affect attachment to cells in addition to inhibiting fusion (Fig. 3), although this requires experimental confirmation and the identification of a bona fide CHIKV receptor. The greatest overlap between the predicted receptor binding site and the Fab footprint occurs for Fab 5M16, although even the close proximity of Fab 4J21 might hinder sterically potential receptor engagement by CHIKV E2. Most of the complementarity determining regions (CDRs) of the Fab molecules interact with the VLP (Table S5). Only the CDR-L2 of Fab 5M16, the Fab with the largest footprint, does not interact with the VLP.

To identify the most important residues on E2 within the Fab binding footprint, we tested alanine mutations throughout this glycoprotein for loss of antibody reactivity (35). MAb binding was assessed against a "shotgun mutagenesis" mutation library of CHIKV E1-E2 mutations with 910 target residues mutated. The entire mutation library was transfected into human HEK-293T cells in a 384-well array format (one clone per well) and assessed for immune reactivity using high-throughput flow cytometry. Residues contributing to each mAb interaction were initially identified as those where mutations resulted in less than 50% reactivity for the mAb of interest (relative to WT CHIKV E1-E2). The residues that resulted in loss of Fab reactivity are consistent with the cryo-EM results (Table S6 and Fig. 4). In addition, some solvent-inaccessible residues near the cryo-EM footprints (Fig. 4) were also identified as affecting Fab reactivity. Presumably, alanine substitutions at these residues induce local conformational changes on the virion surface that impact antibody binding reactivity.

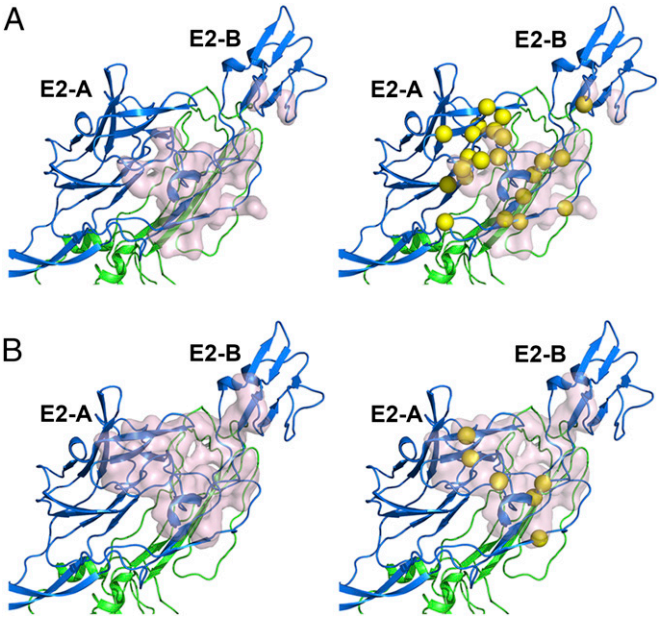

Fig. 4. Comparison of the cryo-EM and alanine scanning mutagenesis mapping for the VLP-4J21 complex and the VLP-5M16 complex. The residues in the cryo-EM epitopes of 4J21 (*A*) and 5M16 (*B*) are surrounded by pink surfaces. The residues identified by alanine scanning are represented by yellow spheres around the relevant Cα atoms. E1 is in green and E2 is in blue.

For the most important residues of the epitope, single mutation of V169A, K234A, or I255A on the E2 β-ribbon connector resulted in complete loss of binding reactivity of mAb 4J21 (<10% reactivity). However, no single alanine mutation on E2 abolished the binding of mAb 5M16. Comparatively, the alanine scanning mutagenesis assays showed that single mutations on E2 had less impact on binding reactivity of 5M16 compared with 4J21. There were only a few residues, when substituted by alanine, which attenuated the binding reactivity of 5M16 by more than 50%. This observation might be because the binding interaction of 5M16 is spread over as many as 29 different residues in the cryo-EM structure of the VLP–5M16 complex.

Comparison of Neutralization of Fab and MAb. Because the valency of binding of mAbs can impact their inhibitory activity (36), we tested the relative neutralizing activity of Fab fragments and IgG against CHIKV infection. The EC_{50} values of the 4J21 and 5M16 Fab molecules were of the same magnitude as the corresponding IgG molecules, demonstrating that cross-linking of envelope proteins or virus aggregation is unlikely to contribute substantially to the neutralization activity. Both the Fab and IgG forms of the 4J21 and 5M16 antibodies neutralized CHIKV at low concentrations within a range of less than 30 ng/mL (Fig. 5).

Among all other human antibodies that have been characterized (35), 5M16 showed the strongest neutralizing activity against CHIKV with EC_{50} values of 3.4 ng/mL for IgG and 5.4 ng/mL for Fab. This potency is similar to that observed with CHK-152 murine antibody (22), which has EC_{50} values of 2 and 13 ng/mL for IgG and Fab molecules, respectively. Although the orientations of the murine and human Fabs are similar relative to the virion surface (Fig. 6), their footprints are different. It is therefore not surprising that their potencies are also different. Despite different orientations, the footprint of the murine Fab CHK-152, like the human Fab 5M16, spans the A and B domains and β-ribbon connector of E2 and

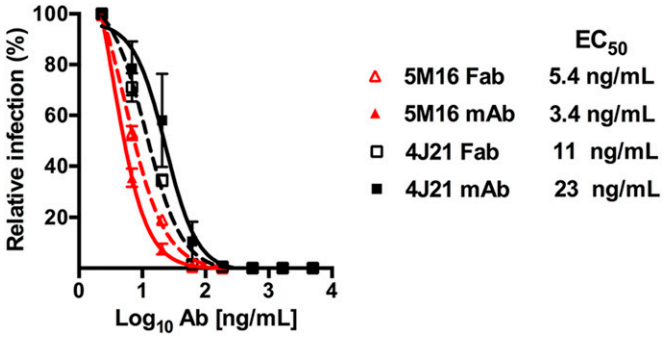

Fig. 5. Neutralization of CHIKV by the IgG and Fab fragments of 4J21 and 5M16. CHIKV neutralization by 4J21 or 5M16 IgG (solid lines) and Fab (dashed lines) as determined in Vero cells. The results are representative of three independent experiments.

therefore inhibits motion of the B domain away from the fusion peptide on E1–DII. Thus, possibly, binding of Fab also results in inhibiting attachment of cellular receptor to the E2–A domain. Both CHK152 and 5M16 have the highest potency among the available murine and human antibodies.

Conclusion

A prior study showed that the 4J21 and 5M16 mAbs had therapeutic activity in immunodeficient mice and inhibited viral fusion with target cell membranes (35). These observations are consistent with the structural results reported here, in that the footprint of Fab 5M16 covers a large area on the surface of the virus. MAb 5M16 stabilized the B domain, which could inhibit fusion by keeping the fusion loop on E1 confined and unexposed beneath the E2–B domain. The footprint of Fab 4J21 covers an area primarily associated with the β-ribbon connector, which keeps the B domain close to the A domain on the viral surface, as well as small regions on the E2–A and E2–B domains. Although Fab 4J21 had less impact on the E2–B domain flexibility, this antibody likely inhibits fusion because it tethers the B domain close to the viral surface by binding to the E2 β-ribbon connector, which normally functions to limit B domain movements.

Materials and Methods

Cells and Viruses. Vero cells (ATCC CCL-81) and HEK293T cells (ATCC CRL-N268) were cultured in DMEM supplemented with 5–10% FBS (Omega Scientific). The CHIKV VLP was purified from FreeStyle 293-F cells (Life Technologies). The human hybridoma cells producing the human mAb 4J21 and 5M16 were isolated previously using human B cells obtained from an immune donor following informed consent, with approval of the Vanderbilt University Medical Center Institutional Review Board (35).

Preparation of CHIKV VLPs and Fab Fragments. The CHIKV VLPs were prepared in PBS (pH 7.4) at a concentration of 2 mg/mL following previously described procedures (20). The human mAbs were purified from the supernatants of cultured human hybridoma cells secreting mAbs, as described previously (35). The Fab fragments were generated by papain digestion of the IgG antibodies using a commercial kit (Thermo Scientific). The Fab fragments were purified further by a Superdex 75 size exclusion column, eluted in PBS buffer (pH 7.4), and concentrated to 5 mg/mL.

Crystallization, Data Collection, and Structure Determination of Fabs. The buffer for the Fab fragments was exchanged to 20 mM Hepes-Na (pH 7.5) before crystallization. Crystals were obtained by using the hanging-drop vapor diffusion method. The 4J21 Fab fragments were crystallized in 24% (wt/vol) PEG 2000, 0.1 M Tris·HCl (pH 8.5), and 0.2 M ammonium acetate. The 5M16 Fab fragments were crystallized in 24% (wt/vol) PEG 3350, 0.1 M Tris·HCl (pH 8.5), and 0.5 M ammonium formate. Crystals were flash frozen in liquid nitrogen. Cryo-protection was achieved by raising the glycerol concentration stepwise to 15% in 5% (vol/vol) increments.

X-ray diffraction data were collected at 100 K at the Advanced Photon Source (APS) beamlines 14BM-C and 23ID-B. Data were indexed and scaled using the HKL2000 (37) and XDS programs (38) (Table S1). The 4J21 and 5M16 crystals diffracted to 2.3- and 2.1-Å resolution, respectively. The space groups were determined as $P2_1$ and $P4_1$, respectively. The Fab structures were determined by molecular replacement with the program Phaser (39). The molecular replacement search molecules were Protein Data Bank (PDB) ID code 3UJT for the variable domain and PDB ID code 4JY6 for the constant domain. The atomic models were built manually using the program Coot (40). The structures were refined further using the program PHENIX (41).

Cryo-EM Sample Preparation, Data Collection, and Single Particle Reconstruction. Fab molecules were mixed with CHIKV VLPs in a 2:1 (Fab: E2) molar ratio. The mixture was incubated on ice for 1 h. Samples were flash-frozen on holey carbon grids in liquid ethane using the Cryo-plunge 3 (CP3) plunger. CCD images of the VLP-4J21 and VLP-5M16 complexes were taken on an FEI Titan Krios electron microscope at a magnification of 37,000× and an electron dosage of ∼20 e/Å^2. All cryo-EM images were collected at about 1.5–3 μm below the focus level.

Particles were selected manually with the e2boxer program in EMAN2 (42). Contrast levels of micrographs were corrected using the ctfit program in EMAN (43). For the reconstructions of VLP-4J21 and VLP-5M16, initial orientations of the particles were assigned with a "random start" model (44), and iterative refinement cycles then were performed to convergence using the jspr program (44). A total of 3,149 and 3,090 particles were used for the reconstruction of the VLP-4J21 and VLP-5M16 complexes, respectively. The final resolution of these reconstructions was 16.5 and 16.8 Å, respectively, using a Fourier shell correlation criterion of 0.5 between two equally sized sets of images that had been kept completely apart from the outset (gold standard).

Structure Fitting and Analysis. The crystal structure of the CHIKV E1–E2 heterodimer (PDB ID code 3N42) (25) was fitted into the cryo-EM density maps as a rigid body, assuming T = 4 symmetry, using the EMfit program (45). The quasi-symmetry operators were initially the same as those used in previous studies of SINV (46) and CHIKV (22) but then were refined further by EMfit during the fitting procedure. The cryo-EM density was set to zero at all grid points within 3 Å of any atom in the final fitted E1–E2 heterodimer. The crystal structures of the 4J21 and 5M16 Fabs were next fitted into the respective modified electron density maps, again assuming T = 4 symmetry. The fitting operations maximized the average density taken over all atomic positions of the quasi-T = 4 related molecules in an icosahedral asymmetric unit while minimizing the clashes between icosahedrally related and quasi-symmetry related atoms, as well as minimizing the number of atoms in low density. Because the 4J21 Fab crystals had two molecules in the asymmetric unit, which had slightly different elbow angles, each of the structural models were fitted independently into the cryo-EM map and only the better fitting structure (Tables S2 and S3), namely the structure with the smaller elbow

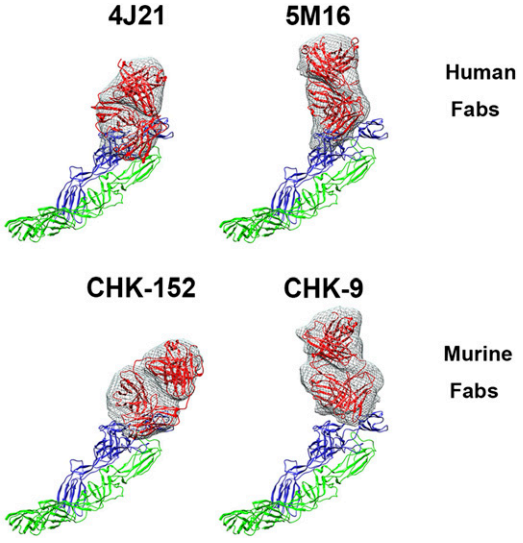

Fig. 6. Comparison of the human and murine Fab molecules bound to the E1–E2 heterodimer. The Fab structures are shown in red and fitted into the cryo-EM density. E1 is shown in green, and E2 is shown in blue.

angle, was chosen and used for the following analysis. Structure analyses were performed using the program Chimera (www.cgl.ucsf.edu/chimera) and PyMOL (The PyMOL Molecular Graphics System, Version 1.7.4; Schrödinger). The contact surface areas between E2 and Fab fragments were calculated by the program PISA (47). The footprints of the Fab fragments on the viral surface were generated by the program RIVEM (48).

Virus Neutralization Assays. Serial dilutions of IgGs or their Fab fragments were incubated with 200 focus-forming units of CHIKV (CHIKV La Reunion 2006 OPY-1) for 1 h at 37 °C. IgG– or Fab–virus complexes were added to Vero cells in 96-well plates. After 120 min, cells were overlaid with 1% (wt/vol) methylcellulose in MEM supplemented with 4% FBS. Plates were harvested 18 h later and fixed with 1% paraformaldehyde in PBS. The plates were incubated sequentially with 500 ng/mL of mouse antibody CHK-9 (30) and HRP-conjugated goat anti-mouse IgG in PBS supplemented with 0.1% saponin and 0.1% BSA. CHIKV-infected foci were visualized using TrueBlue peroxidase substrate (KPL), quantitated on an ImmunoSpot 5.0.37 macroanalyzer (Cellular Technologies Ltd), and analyzed using GraphPad Prism software.

Alanine-Scanning Mutagenesis and Immunofluorescence-Based Binding Assay. A CHIKV envelope protein expression construct (strain S27; Uniprot Reference Q8JUX5) with a C-terminal V5 tag was subjected to alanine-scanning mutagenesis to generate a comprehensive mutation library, as described previously (28, 35). Primers were designed to mutate each residue within the E2, 6K, and E1 regions of the envelope proteins to alanine, except for alanine codons, which were mutated to serine. In total, 910 CHIKV envelope protein mutants were generated and transiently expressed in HEK293T cells for 22 h in 384-well plates. Cells expressing the protein mutants were fixed in 4% paraformaldehyde in PBS plus calcium and magnesium ($PBS^{+/+}$) and stained sequentially with 0.375–0.5 μg/mL of monoclonal monoclonal antibodies and 7.5 μg/mL AlexaFluor488-conjugated goat anti-human IgG $F(ab')_2$ secondary antibody (Jackson ImmunoResearch) diluted in 10% normal goat serum (NGS). Mean cellular fluorescence was recorded using a high-throughput flow cytometer (HTFC; Intellicyt). Antibody reactivity against each mutant relative to the WT protein was calculated by subtracting the signal from mock-transfected controls and normalizing to the signal from WT-transfected controls.

ACKNOWLEDGMENTS. We thank Sheryl Kelly for help with the manuscript preparation and Valorie Bowman for technical support with the electron microcopy. We also thank the staff of beamlines 14BM-C and 23ID-B at the Advanced Photon Source of Argonne National Laboratory for help in data collection. Use of the Advanced Photon Source, an Office of Science User Facility operated for the US Department of Energy (DOE) Office of Science by Argonne National Laboratory, was supported by US DOE Contract DE-AC02-06CH11357. This work was supported by National Institutes of Health (NIH) Grant R01 AI095366 (to M.G.R.), NIH Grant R01 AI089591 (to M.S.D.), NIH Contract HHSN272200900055C (to B.J.D.), and NIH Grant R01 AI114816 (to J.E.C. and M.S.D.).

1. Griffin DE (2007) Alphaviruses. *Fields Virology*, eds Knipe DM, Howley PM (Lippincott Williams & Wilkins, Philadelphia), 5th Ed, pp 1023–1067.
2. Kuhn RJ (2007) *Togaviridae*: The viruses and their replication. *Fields Virology*, eds Knipe DM, Howley PM (Lippincott Williams & Wilkins, Philadelphia), 5th Ed, pp 1001–1022.
3. Schilte C, et al. (2013) Chikungunya virus-associated long-term arthralgia: A 36-month prospective longitudinal study. *PLoS Negl Trop Dis* 7(3):e2137.
4. Staples JE, Breiman RF, Powers AM (2009) Chikungunya fever: An epidemiological review of a re-emerging infectious disease. *Clin Infect Dis* 49(6):942–948.
5. Robinson MC (1955) An epidemic of virus disease in Southern Province, Tanganyika Territory, in 1952-1953. *Trans R Soc Trop Med Hyg* 49:28–32.
6. Thiboutot MM, et al. (2010) Chikungunya: A potentially emerging epidemic? *PLoS Negl Trop Dis* 4(4):e623.
7. Powers AM, Logue CH (2007) Changing patterns of chikungunya virus: Re-emergence of a zoonotic arbovirus. *J Gen Virol* 88(Pt 9):2363–2377.
8. Centers for Disease Control and Prevention (2015) NOWCAST: Chikungunya in the Americas. Available at www.cdc.gov/chikungunya/modeling/index.html. Accessed July 11, 2015.
9. Mukhopadhyay S, et al. (2006) Mapping the structure and function of the E1 and E2 glycoproteins in alphaviruses. *Structure* 14(1):63–73.
10. Kielian M (2006) Class II virus membrane fusion proteins. *Virology* 344(1):38–47.
11. Gibbons DL, et al. (2003) Visualization of the target-membrane-inserted fusion protein of Semliki Forest virus by combined electron microscopy and crystallography. *Cell* 114(5):573–583.
12. Simizu B, Yamamoto K, Hashimoto K, Ogata T (1984) Structural proteins of Chikungunya virus. *J Virol* 51(1):254–258.
13. Ivanova L, Le L, Schlesinger MJ (1995) Characterization of revertants of a Sindbis virus 6K gene mutant that affects proteolytic processing and virus assembly. *Virus Res* 39(2-3):165–179.
14. Lobigs M, Zhao HX, Garoff H (1990) Function of Semliki Forest virus E3 peptide in virus assembly: Replacement of E3 with an artificial signal peptide abolishes spike heterodimerization and surface expression of E1. *J Virol* 64(9):4346–4355.
15. Ziemiecki A, Garofff H (1978) Subunit composition of the membrane glycoprotein complex of Semliki Forest virus. *J Mol Biol* 122(3):259–269.
16. Zhang R, et al. (2011) 4.4 Å cryo-EM structure of an enveloped alphavirus Venezuelan equine encephalitis virus. *EMBO J* 30(18):3854–3863.
17. Garcea RL, Gissmann L (2004) Virus-like particles as vaccines and vessels for the delivery of small molecules. *Curr Opin Biotechnol* 15(6):513–517.
18. Ludwig C, Wagner R (2007) Virus-like particles-universal molecular toolboxes. *Curr Opin Biotechnol* 18(6):537–545.
19. Roldão A, Mellado MC, Castilho LR, Carrondo MJ, Alves PM (2010) Virus-like particles in vaccine development. *Expert Rev Vaccines* 9(10):1149–1176.
20. Akahata W, et al. (2010) A virus-like particle vaccine for epidemic Chikungunya virus protects nonhuman primates against infection. *Nat Med* 16(3):334–338.
21. Chang LJ, et al.; VRC 311 Study Team (2014) Safety and tolerability of chikungunya virus-like particle vaccine in healthy adults: A phase 1 dose-escalation trial. *Lancet* 384(9959):2046–2052.
22. Sun S, et al. (2013) Structural analyses at pseudo atomic resolution of Chikungunya virus and antibodies show mechanisms of neutralization. *eLife* 2:e00435.
23. Lescar J, et al. (2001) The Fusion glycoprotein shell of Semliki Forest virus: An icosahedral assembly primed for fusogenic activation at endosomal pH. *Cell* 105(1):137–148.
24. Rey FA, Heinz FX, Mandl C, Kunz C, Harrison SC (1995) The envelope glycoprotein from tick-borne encephalitis virus at 2 A resolution. *Nature* 375(6529):291–298.
25. Voss JE, et al. (2010) Glycoprotein organization of Chikungunya virus particles revealed by X-ray crystallography. *Nature* 468(7324):709–712.
26. Li L, Jose J, Xiang Y, Kuhn RJ, Rossmann MG (2010) Structural changes of envelope proteins during alphavirus fusion. *Nature* 468(7324):705–708.
27. Smith TJ, et al. (1995) Putative receptor binding sites on alphaviruses as visualized by cryoelectron microscopy. *Proc Natl Acad Sci USA* 92(23):10648–10652.
28. Fong RH, et al. (2014) Exposure of epitope residues on the outer face of the chikungunya virus envelope trimer determines antibody neutralizing efficacy. *J Virol* 88(24):14364–14379.
29. Kam YW, et al. (2012) Longitudinal analysis of the human antibody response to Chikungunya virus infection: Implications for serodiagnosis and vaccine development. *J Virol* 86(23):13005–13015.
30. Pal P, et al. (2013) Development of a highly protective combination monoclonal antibody therapy against Chikungunya virus. *PLoS Pathog* 9(4):e1003312.
31. Selvarajah S, et al. (2013) A neutralizing monoclonal antibody targeting the acid-sensitive region in chikungunya virus E2 protects from disease. *PLoS Negl Trop Dis* 7(9):e2423.
32. Warter L, et al. (2011) Chikungunya virus envelope-specific human monoclonal antibodies with broad neutralization potency. *J Immunol* 186(5):3258–3264.
33. Hernandez R, Paredes A, Brown DT (2008) Sindbis virus conformational changes induced by a neutralizing anti-E1 monoclonal antibody. *J Virol* 82(12):5750–5760.
34. Porta J, et al. (2014) Locking and blocking the viral landscape of an alphavirus with neutralizing antibodies. *J Virol* 88(17):9616–9623.
35. Smith SA, et al. (2015) Isolation and characterization of broad and ultrapotent human monoclonal antibodies with therapeutic activity against Chikungunya virus. *Cell Host Microbe* 18(1):86–95.
36. Edeling MA, et al. (2014) Potent dengue virus neutralization by a therapeutic antibody with low monovalent affinity requires bivalent engagement. *PLoS Pathog* 10(4):e1004072.
37. Otwinowski Z, Minor W (1997) Processing of X-ray diffraction data collected in oscillation mode. *Methods in Enzymology*, ed Carter, Jr CW (Academic Press, New York), Vol 276, pp 307–326.
38. Kabsch W (2010) Xds. *Acta Crystallogr D Biol Crystallogr* 66(Pt 2):125–132.
39. McCoy AJ, et al. (2007) *Phaser* crystallographic software. *J Appl Cryst* 40(Pt 4):658–674.
40. Emsley P, Cowtan K (2004) Coot: Model-building tools for molecular graphics. *Acta Crystallogr D Biol Crystallogr* 60(Pt 12 Pt 1):2126–2132.
41. Adams PD, et al. (2010) PHENIX: a comprehensive Python-based system for macromolecular structure solution. *Acta Crystallogr D Biol Crystallogr* 66(Pt 2):213–221.
42. Tang G, et al. (2007) EMAN2: An extensible image processing suite for electron microscopy. *J Struct Biol* 157(1):38–46.
43. Ludtke SJ, Baldwin PR, Chiu W (1999) EMAN: Semiautomated software for high-resolution single-particle reconstructions. *J Struct Biol* 128(1):82–97.
44. Guo F, Jiang W (2014) Single particle cryo-electron microscopy and 3-D reconstruction of viruses. *Electron Microscopy, Methods and Protocols*, ed Kuo J (Humana Press, Springer, New York), 3rd Ed, pp 401–443.
45. Rossmann MG, Bernal R, Pletnev SV (2001) Combining electron microscopic with x-ray crystallographic structures. *J Struct Biol* 136(3):190–200.
46. Rossmann MG, Blow DM (1962) The detection of sub-units within the crystallographic asymmetric unit. *Acta Crystallogr* 15:24–31.
47. Krissinel E, Henrick K (2007) Inference of macromolecular assemblies from crystalline state. *J Mol Biol* 372(3):774–797.
48. Xiao C, Rossmann MG (2007) Interpretation of electron density with stereographic roadmap projections. *J Struct Biol* 158(2):182–187.